

Published in final edited form as:

*Neuroimage*. 2012 January 16; 59(2): 1132–1142. doi:10.1016/j.neuroimage.2011.06.066.

## Correlation and heritability in neuroimaging datasets: A spatial decomposition approach with application to an fMRI study of twins

Joonkoo Park<sup>1</sup>, Kerby Shedden<sup>2</sup>, and Thad A. Polk<sup>1</sup>

<sup>1</sup>Department of Psychology, University of Michigan

<sup>2</sup>Department of Statistics, University of Michigan

### Abstract

Advances in modern neuroimaging in combination with behavioral genetics have allowed neuroscientists to investigate how genetic and environmental factors shape human brain structure and function. Estimating the heritability of brain structure and function via twin studies has become one of the major approaches in studying the genetics of the brain. In a classical twin study, heritability is estimated by computing genetic and phenotypic variation based on the similarity of monozygotic and dizygotic twins. However, heritability has traditionally been measured for univariate, scalar traits, and it is challenging to assess the heritability of a spatial process, such as a pattern of neural activity. In this work, we develop a statistical method to estimate phenotypic variance and covariance at each location in a spatial process, which in turn can be used to estimate the heritability of a spatial dataset. The method is based on a dimensionally-reduced model of spatial variation in paired images, in which adjusted least squares estimates can be used to estimate the key model parameters. The advantage of the proposed method compared to conventional methods such as a voxelwise or mean-ROI approaches is demonstrated in both a simulation study and a real data study assessing genetic influence on patterns of brain activity in the visual and motor cortices in response to a simple visuomotor task.

### Keywords

Heritability; Intraclass Correlation; Twin Study; Spatial Analysis; Genetics

### Introduction

In a classical twin study, the heritability of a trait is assessed by estimating genetic and phenotypic variation based on the similarity (i.e. intraclass correlation) of monozygotic (MZ) and dizygotic (DZ) twins. Conventionally, heritability is measured for univariate, scalar traits (e.g. IQ, body mass index, etc.); however, there are cases where the trait is defined by a spatial process (e.g. a pattern of neural activation estimated from neuroimaging studies). For example, a number of neuroimaging studies have studied twins in order to

---

© 2011 Elsevier Inc. All rights reserved.

Correspondence should be addressed to: Joonkoo Park, joonkoo@umich.edu, 530 Church St. Ann Arbor, MI 48109, Phone: (734) 763-0343, Fax: (734) 763-7480.

**Publisher's Disclaimer:** This is a PDF file of an unedited manuscript that has been accepted for publication. As a service to our customers we are providing this early version of the manuscript. The manuscript will undergo copyediting, typesetting, and review of the resulting proof before it is published in its final citable form. Please note that during the production process errors may be discovered which could affect the content, and all legal disclaimers that apply to the journal pertain.

investigate the heritability of brain structure and function (Blokland et al., 2008; Brun et al., 2009; Cote et al., 2007; Jahanshad et al., 2010; Koten et al., 2009; Lee et al., 2010; Matthews et al., 2007; Polk et al., 2007; Schmitt et al., 2009; Thompson et al., 2001). These studies make structural measurements and/or estimate neural activation at tens of thousands of data points. Even if the researcher restricts the focus of investigation to a smaller region of interest (ROI), these regions still often include hundreds or thousands of voxels. So how we can assess the heritability of a measure that is multivariate and spatial in nature?

One straightforward way is to estimate heritability at each voxel (or vertex) separately. In this approach, images from all twins are first normalized into a standard space. Then, genetic modeling is performed using the classical twin design at each voxel, which provides a measure of heritability at every voxel across the entire brain. This “voxelwise” approach has been used in many studies investigating heritability in structural neuroimaging data (e.g. Thompson et al., 2001). Since the voxelwise approach ignores the spatial relationships among voxels, it does not make the most efficient use of the information in the data. With relatively high signal-to-noise ratio and reliability in high-resolution anatomical images, the voxelwise approach may maintain adequate power for some structural neuroimaging studies. But the voxelwise approach becomes more troublesome in functional neuroimaging studies in which the data typically have much lower signal-to-noise ratio at the voxel level (Huettel et al., 2004), which may result in highly variable estimates, particularly with smaller sample size.

One way to account for the noisy nature of functional neuroimaging data is to restrict heritability estimation to a smaller region of interest (ROI). Except for one study using an extended twin design that maximizes power to detect heritability (Koten et al., 2009), most functional neuroimaging twin studies have adopted the “mean-ROI” approach, in which heritability estimation is based on mean intensity values across voxels within an ROI (Blokland et al., 2008; Cote et al., 2007; Matthews et al., 2007). The mean-ROI approach estimates the heritability of a function of the data (i.e. spatial average) and allows traditional heritability estimation schemes for scalar-valued traits to be applied in an imaging study. If the ROI is functionally homogeneous, averaging intensity values within the ROI increases the signal-to-noise ratio. However, if there are inherent spatial correlations and inhomogeneity within the ROI (which is likely), this approach may result in a significant loss of power (Friston et al., 2006). For example, if only a subregion of the ROI shows heritable activation, this mean-ROI approach would show an intermediate level of heritability at a constant level throughout the ROI. Furthermore, recent fMRI studies have demonstrated that multivariate spatial patterns can contain unique information over and above univariate intensity values (Haynes & Rees, 2006; Norman et al., 2007).

Finally, it is possible to assess genetic influences on a spatially measured trait using statistical association measures that are not directly related to heritability. For example, Polk et al., (2007) considered the correlation across voxels within each twin pair, and compared the averages of these correlations for MZ and DZ twin pairs. This provides a quantitative assessment of familiarity using a familiar and stable statistical approach, but does not provide estimates of genetic heritability.

In this work, we develop a statistical method for heritability estimation in functional neuroimaging studies of twins that addresses the main limitation of the mean-ROI method as well as the voxelwise method. The proposed method estimates correlation for MZ and for DZ twin pairs at each position in an ROI (or the whole brain), which in turn are used to estimate heritability. The method for estimating the correlation values is based on a statistical model in which the variation in the measured trait at each spatial position is viewed as arising from a linear combination of spatial basis volumes. In a simulation study,

we report the feasibility of this “spatial decomposition” method and explore its relative advantages compared to the conventional mean-ROI method and the voxelwise method. The relative advantage of the proposed method is also examined in a real fMRI study of a simple visuomotor task. We first assess the role of genetics in the functional neural architecture by comparing the intraclass correlation (ICC) of activation maps from MZ and DZ pairs. We then utilize the proposed spatial decomposition method to estimate the heritability of neural patterns in the visual and motor cortices by incorporating the structural equation model (SEM) approach to estimating heritability (Neale, 1998, 2003).

## Statistical Method

### Overall description

The spatial data  $Y$  for each individual is modeled as a linear combination of basis volumes  $X_p$ , scaled by unobserved random coefficients  $\beta_p$ . The  $X_p$ 's represent underlying spatial patterns for the given phenotypic trait. The  $\beta_p$ 's have unknown mean and variance, and unknown covariance between individuals in a twin pair, but are independent between twin pairs. The goal is to use the model to estimate these variance and covariance parameters, which in turn determine the correlation (or ICC<sup>1</sup>) at each spatial point. As demonstrated below, these parameters can be estimated using fixed effects regression (i.e. ordinary least-squares regression), followed by some additional processing of the fitted regression parameters to account for uncertainty in the fixed effects estimates.

### Model

Let  $Y_{ij}$  represent spatial data from a given ROI (possibly the whole brain) from the  $j$ th twin in the  $i$ th pair ( $i=1 \dots n, j=1,2$ ). For instance,  $Y_{ij}$  can be a vectorized representation of three-dimensional volumetric fMRI data (e.g. contrast maps, percent signal change maps, or t-maps) as a vector of  $v$  elements where  $v$  is the size of the ROI. Conditioning on the  $\beta_p$ 's, the data  $Y_{i1}$  and  $Y_{i2}$  for a single twin pair is then modeled as a linear combination of a number of basis volumes  $X_p$  as follows:

$$\begin{pmatrix} Y_{i1} \\ Y_{i2} \end{pmatrix} = \begin{pmatrix} X_0, X_1 \dots X_p & 0 \\ 0 & X_0, X_1 \dots X_p \end{pmatrix} \cdot \begin{pmatrix} \beta_{0i1} \\ \vdots \\ \beta_{pi1} \\ \beta_{0i2} \\ \vdots \\ \beta_{pi2} \end{pmatrix} + \varepsilon. \quad (1)$$

In this paper, particularly in the subsequent real data study, the basis volumes  $X_p$  were constructed from the neural activation patterns of an independent group of subjects performing the same task. The eigenvectors obtained from a singular value decomposition of these data were used as the basis volumes<sup>2</sup>. This serves to focus the heritability analyses on the more variable spatial components in the data. The coefficients,  $\beta_{pij}$ , are viewed as random variables with unknown mean and variance. The residual,  $\varepsilon$ , is viewed as centered errors uncorrelated across the voxels with constant variance across voxels.

<sup>1</sup>See Appendix for the working definition of intraclass correlation.

<sup>2</sup> $X_0$  is an intercept volume that is created to be orthogonal to the rest of the basis volumes.

## Correlation Estimation

Using the model, we now estimate the voxel-level variance of  $Y_{ij}$ ,  $var(Y_{\bullet j})$ , and the voxel-level covariance between  $Y_{i1}$  and  $Y_{i2}$ ,  $cov(Y_{\bullet 1}, Y_{\bullet 2})$ . That is,  $var(Y_{\bullet j})$  and  $cov(Y_{\bullet 1}, Y_{\bullet 2})$  are both vectors, with as many elements as there are voxels in the ROI. We note that in the conventional voxelwise approach, these variance and covariance values are estimated directly using the usual sample variance and covariance estimators at each voxel separately. We also note that in the conventional mean-ROI approach, the mean  $Y_{ij}$  across the entire ROI is first computed, after which variance and covariance of the mean values are estimated. Our aim here is to use the regression model to improve the precision of these estimates, by borrowing information within spatial regions.

The first step is to use ordinary least squares, applied separately to each twin pair, to predict the  $\beta_{pij}$  values. The model-implied variance,  $var(Y_{\bullet j})$ , and covariance,  $cov(Y_{\bullet 1}, Y_{\bullet 2})$ , can then be estimated as follows:

$$\widehat{var}(Y_{\bullet j}) = \sum_p X_p^2 \widehat{var}(\beta_{p\bullet j}) + \sigma^2 \quad (2)$$

$$\widehat{cov}(Y_{\bullet 1}, Y_{\bullet 2}) = \sum_p X_p^2 \widehat{cov}(\beta_{p\bullet 1}, \beta_{p\bullet 2}), \quad (3)$$

where  $X_p^2$  represents element-wise squares. Here,  $\widehat{var}(\beta_{p\bullet j})$  and  $\widehat{cov}(\beta_{p\bullet 1}, \beta_{p\bullet 2})$  are bias corrected versions of the standard empirical variance and the empirical covariance, respectively (see Appendix). The residual variance ( $\sigma^2$ ) can be estimated from the mean of the error variance across all voxels. The covariance of residuals between pairs is assumed to be zero, and is therefore omitted in Equation 3.

As correlation is defined by the ratio of covariance and variance, the correlation of two spatial patterns can then be estimated by performing element-wise divisions as follows:

$$corr(Y_{\bullet 1}, Y_{\bullet 2}) = \frac{\widehat{cov}(Y_{\bullet 1}, Y_{\bullet 2})}{\sqrt{\widehat{var}(Y_{\bullet 1}) \times \widehat{var}(Y_{\bullet 2})}}. \quad (4)$$

## Genetic Effects and Heritability Estimation

A classical twin study asserts that the variance of a phenotype can be decomposed into additive genetics, common environment, and unique environment with twins that are reared together (Falconer and Mackay, 1996). The comparison between the ICC of MZ pairs and of DZ pairs provides a quick and easy way to assess genetic effects on the phenotypic trait. Since MZ pairs share all of their alleles while DZ twins share 50% on average, phenotypic covariance for MZ twins should be more similar than that of DZ twins if genes account for variation between individuals.

While the comparison between the ICC of MZ twins and DZ twins can be a useful tool to examine the genetic influence in the phenotypic trait, modern covariance modeling methods provide a quantitative estimate of heritability (Christian et al., 1995; Neale, 2003). As described above, the variance  $var(Y_{\bullet j})$  and the sibling covariance  $cov(Y_{\bullet 1}, Y_{\bullet 2})$  can be estimated using the spatial decomposition approach. These values can then be fed into a

maximum-likelihood model-fitting algorithm using structural equation modeling (SEM) implemented in Mx (Neale et al., 2003) in order to estimate genetic and environmental components of phenotypic variance.

## Simulation Study

### Methods

A simulation study was conducted in order to evaluate the model-based point estimates of the correlation parameters in terms of bias, variance, and mean squared error. Patterns of neural activation ( $Y_{ij}$ ) were simulated in a 3-D space of 512 ( $8 \times 8 \times 8$ ) voxels from pairs ( $n = 10, 20, 40$ ) of data as in Equation 1. The set of basis volumes ( $X_0, \dots, X_p$ ) was derived from the eigenvectors of the covariance matrix of the entire voxel space. A rational quadratic covariance function with both parameters equal to 1 was used to determine the spatial structure of the simulated trait data. In this simulation study, we wanted to examine in particular the effect of underspecification (i.e. a model with fewer basis volumes than what was used to construct the full data) and overspecification (i.e. a model with more basis volumes than what was used to construct the full data). Therefore, we arbitrarily decided to use the first 32 eigenvectors of the covariance matrix as the spatial structure of the trait values.

The coefficients for each these 32 basis volumes,  $\beta_{pij}$ , are drawn randomly from a bivariate normal distribution. The mean of this bivariate normal distribution was 0, and the variance was set in a monotonically decreasing order to mimic real data<sup>3</sup>. The covariance of this bivariate random distribution was manipulated so that the correlation was fixed at  $r$ . Various levels of correlation between 0 and 1 were considered in order to examine the effect of similarity between pairs on the point estimates. The errors ( $\epsilon$ ) were drawn from a normal distribution with mean of zero and standard deviation of  $\sigma$ , which was set at various values between 0 and 1.

For each case in the parameter space, simulated data were generated 500 times and the correlation was estimated for each sample using three different methods. Firstly, the correlation was estimated using the proposed spatial decomposition method. Here, five different types of models were used to estimate the correlation. Note that the simulated data were generated based on 32 basis volumes. In five different models, the first 4, the first 8, the first 16, the first 32, and the first 64 (i.e. including all the basis volumes used in the simulated data but also 32 more basis volumes from the initial set of eigenvectors) were used, respectively, to estimate the correlation. In the first three cases, the model is underspecified in terms of the basis volumes, and in the last case, the model is overspecified. Secondly, the correlation was estimated using the conventional voxelwise method. Thirdly, the correlation was estimated using the mean-ROI approach, in which mean values of the entire voxel space for pairs were correlated.

In all three of these methods, the mean root squared error (RMSE), root integrated squared bias (RISB), and integrated variance (IVAR) were computed by comparing the simulated results and the voxel-level true correlation. Given the parameters  $r$  and  $\sigma$  and the basis volumes that went into simulating the data, the true voxel-level correlation at each voxel can be computed from Equation 4. Then, RMSE between the estimated correlation and the true correlation was computed at every repetition, and the mean RMSE over 500 repetitions was computed. The variance of the correlation estimates over 500 repetitions at each voxel was also computed, and the integrated variance (IVAR) was measured by computing the mean of

<sup>3</sup>That is, the variance of the coefficients associated with  $p$ th basis volume was exponentially decreasing defined as  $\exp(33-p) / \exp(32) \times 3,000$ , where  $p = 1, 2, \dots, 32$ .

these variance measures across all voxels. Likewise, the mean of the correlation estimates over 500 repetitions was compared with the true correlation, which resulted in root integrated squared bias (RISB).

## Results

Figure 1 illustrates RMSE, IVAR, and RISB of the correlation estimates from three different methods simulating data from 20 pairs<sup>4</sup>. Similar RMSE values were observed among the results from the five different model fitting approaches in the spatial decomposition method. However, a closer look at RISB revealed some systematic patterns in underspecified ( $P=4, 8, \text{ or } 16$ ) models. That is, RISB increased (particularly when  $r$  was high) as the model was more underspecified, although this reduced RISB was not visually observable after  $P=8$ . There were no visually observable effects of overspecification at least in this parameter space. In general, RISB remained low in the entire parameter space, which indicates that the bias introduced when estimating the ratio between two unbiased estimates (the numerator and denominator of Equation 4) is small in the setting of this simulation study (see Stuart and Ord, 2009).

The results from the voxelwise method and the mean-ROI method demonstrate that RMSE from these two methods is larger than RMSE from the spatial decomposition method. This increase was driven by larger RISB and IVAR in both methods compared to the spatial decomposition method (except in the cases when the model was extremely underspecified). There was a slight advantage of reduced IVAR in the mean-ROI method (average IVAR across the parameter space was 0.0294) compared to the voxelwise method (average IVAR was 0.0300). The mean-ROI approach resulted in much greater RISB than the voxelwise method (particularly when  $\sigma$  and  $r$  were high).<sup>5</sup>

## Real Data Study

### Method

**Participants**—Thirteen pairs of right-handed MZ twins (nine female pairs, four male pairs, ages 18-29 with a mean age of 21.3) and eleven pairs of DZ twins (seven female pairs, four male pairs, ages 18-23, mean age 19.9) reared together participated in the study. Zygosity was determined by comparing seven to eight highly variable DNA markers (D5S818, D13S317, D7S820, D16S539, vWA, TH01, TPOX, CSF1PO) from the buccal cells of twins collected by swabbing the cheek of each participant. DNA was amplified using the polymerase chain reaction technique. Twins in whom all the markers matched were classified as monozygotic and twins in whom some markers mismatched were classified as dizygotic. Additionally, data from an independent group of nineteen subjects (12 females, ages 18-23, mean age of 19.9) were collected.

**Experimental Procedure and Data Acquisition**—During a functional MRI session, participants performed a simple visuomotor task. Participants were instructed to fixate on the “+” at the center of the screen. Every 16 seconds, a circular checkerboard flickered at the rate of 8 Hz at the center of the screen for 2 seconds, and the participants were asked to press a button once with the right index finger as soon as they saw the flickering checkerboard. This session lasted for five minutes.

High-resolution T1-weighted anatomical images were collected in a GE 3T scanner using spoiled-gradient-recalled acquisition (SPGR) in axial slices parallel to the AC/PC line with a

<sup>4</sup>See Supplementary Figure S1 for results with 10 and 40 pairs.

<sup>5</sup>See Supplementary Figure S2 for a discussion about the bias in the mean-ROI method.

resolution of  $0.9375 \times 0.9375 \times 5.0$  mm. Neural activity was estimated based on the blood-oxygen level dependent (BOLD) signal using a spiral acquisition sequence with the following parameters: TR = 2000 ms, TE = 30 ms, flip angle =  $90^\circ$ , slice thickness = 5 mm, in-plane resolution =  $3.75 \times 3.75$  mm, number of slices = 30, and field of view = 24cm.

**Preprocessing and Data Modeling**—The functional images for each participant underwent reconstruction, slice timing correction, and realignment as part of preprocessing. The high-resolution anatomical image for each participant was coregistered to the mean of all functional images. Then, the anatomical image was segmented using SPM8 (Wellcome Department of Cognitive Neurology, London) to separate gray and white matter voxels using the International Consortium of Brain Mapping (ICBM) tissue probability maps, and affine normalization parameters were calculated from those maps in standard MNI space. The functional images for each individual were then normalized to the template space with a resolution of  $3 \times 3 \times 3$  mm and spatially smoothed with a Gaussian kernel of  $8 \times 8 \times 8$ mm.

We followed a conventional voxel-by-voxel approach for reducing the temporal data to a single activation map. For each participant, a general linear model (GLM) corrected for temporal autocorrelation (using an AR(1) model) with regressors corresponding to the experimental condition (i.e. presentation of the flickering checkerboard) using SPM8. The resulting parameter estimates of the GLM, henceforth referred to as the activation maps, were used in further analyses.

**Regions of Interest**—The regions of interest (ROIs) were defined in the left visual cortex, right visual cortex, and the left motor cortex. The left and right visual cortices were constructed as the union of the calcarine sulcus, lingual gyrus, and cuneus separately in the left and the right hemisphere using the PickAtlas AAL software toolbox (Maldjian et al., 2003; Tzourio-Mazoyer et al., 2002). The left motor cortex was constructed as the pre-central gyrus from the same toolbox. These three masks were resliced to match the voxel space of the functional data. This procedure resulted in a mask with 783 voxels in the left visual cortex, 913 voxels in the right visual cortex, and 428 voxels in the left motor cortex.

**Intraclass Correlation Differences**—The brain activation maps within the left and the right visual cortex from an independent group of nineteen subjects were mean-centered and underwent singular value decomposition which resulted in nineteen eigenvectors. These eigenvectors served as the basis volumes of the given neural pattern elicited by the visuomotor task within the two masks. Then, the brain activation maps from twin participants were entered into the proposed model (Eq. 1) separately for MZ twin pairs and DZ twin pairs. After fixed effects regression and a bias correction procedure (see Statistical Model), the variances and covariances of the  $\beta$  values were estimated (see Equation 2 and 3) from which the ICC for each twin group was estimated<sup>6</sup>. The estimated error standard deviation,  $\sigma$ , was 0.686 (left visual), 0.823 (right visual), and 0.435 (left motor) in MZ pairs and 0.547 (left visual), 0.606 (right visual), and 0.393 (left motor) in DZ pairs.

There were no significant effects of age ( $b=0.0591$ ,  $p=0.429$  in the left visual cortex;  $b=0.0246$ ,  $p=0.783$  in the right visual cortex;  $b=0.0883$ ,  $p=0.073$  in the left motor cortex) or sex ( $b=0.4200$ ,  $p=0.278$  in the left visual cortex;  $b=0.2668$ ,  $p=0.566$  in the right visual cortex;  $b=0.2144$ ,  $p=0.410$  in the left motor cortex) on the mean activation values across all subjects, and therefore the activation maps were not adjusted for age or sex when estimating ICC.

<sup>6</sup>ICC is truncated at zero if negative.

ICC maps of MZ and DZ pairs<sup>7</sup> were then compared by taking the difference between the two,  $ICC_{MZ} - ICC_{DZ}$ . If there is genetic influence on the neural activation pattern, then the difference map should be positive. Regions with positive differences were identified, and the statistical significance of the cluster size was computed based on a clusterwise correction for multiple comparisons (Holmes et al., 1996; Nichols & Holmes, 2002). To be specific, a simulation was used to derive the distribution of the maximum cluster size under the null hypothesis. The null distribution, under the assumption that there is no difference between the  $ICC_{MZ}$  and  $ICC_{DZ}$ , was constructed by permuting the zygosity label of each twin pair (Chiang et al., 2008). First, a heritability map was derived from many repetitions (10,000) while permuting the zygosity. At each repetition, clusters of heritable regions were defined by contiguous voxels exceeding a certain magnitude threshold (i.e. the top 95 percentile value). The volume of the largest cluster defined at this magnitude threshold level was recorded after each repetition, and these measures served as the null distribution of the size of the cluster at a given threshold.

**Heritability**—Heritability of the neural activation pattern was estimated using a maximum-likelihood model fitting approach via SEM (using the Mx software). Variance maps (Eq. 2) and covariance maps (Eq. 3) were constructed<sup>8</sup> from twins separately for MZ and DZ pairs using the proposed spatial decomposition method. The variance and covariance measures at each voxel were fit to a univariate AE model to estimate additive genetic (A) and unique environmental (E) contributions to the variation in the neural activation pattern (see Voxelwise Method below for the motivation for an AE model). Heritability ( $h^2$ ) was defined as the proportion of variance from all components (additive genetics and unique environmental, A+E) that was explained by additive genetics (A) alone. As in the case of identifying regions showing greater  $ICC_{MZ}$  than  $ICC_{DZ}$  within the bilateral visual cortex, clusterwise correction for multiple comparisons incorporating permutation (1,000) was used to assess significantly heritable regions within the visual cortex.

**Voxelwise Method**—ICC difference and heritability was also estimated using the conventional voxelwise method. More specifically, ICC was computed at each voxel separately for MZ twin pairs and DZ twin pairs<sup>9</sup>, and the difference between the resulting ICC maps was computed. For the voxelwise estimation of heritability, variance and covariance measures were computed at each voxel, then heritability was estimated at each voxel initially using the ACE model in Mx. The ACE model, however, returned negligible estimation of common environmental effect in many of the voxels (73.6% of the voxels in the left visual ROI, 71.3% of the voxels in the right visual ROI, and 64.0% of the voxels in the left motor ROI). In addition, the observation of the  $ICC_{MZ}$  and  $ICC_{DZ}$  maps revealed that  $ICC_{DZ}$  was less than half of  $ICC_{MZ}$  in the majority of voxels. Thus, an AE model was fit for parsimony. As in the case of the spatial decomposition method, statistical inference on the ICC difference and heritability was made using a clusterwise correction for multiple comparisons.

**Mean-ROI Method**—Lastly, ICC difference and heritability were estimated using the conventional mean-ROI method. Neural activity values were averaged across all the voxels within each ROI, and these summary measures were used in the subsequent ICC and heritability estimation. As in the other methods, an AE model was used for heritability estimation, and the statistical significance of the estimates was assessed using the permutation method.

<sup>7</sup>See Supplementary Figures S3 and S4 for ICC maps of MZ and DZ pairs computed using the spatial decomposition method.

<sup>8</sup>Conventional variance and covariance were used with appropriate bias correction instead of the covariance and variance formula used in Fisher's ICC.

<sup>9</sup>See Supplementary Figures S5 and S6 for ICC maps of MZ and DZ pairs computed using the voxelwise method.

**Residual Diagnostics**—The model (Eq. 1) assumes that the errors are spatially unstructured, or at least contain no covarying information between pairs. In practice, however, it is possible that some spatially defined covarying information is not fully captured by the given basis volumes. This is particularly likely when the model is underspecified as shown in the simulation study. In the data from the real study, we empirically tested how much covarying information was left in the errors. Residual maps for individual twins were constructed. Then the intraclass correlation of the residual values between twins across pairs was computed at each voxel. If there is no covarying information left in the errors, we should expect negligible correlation across all voxels on average.

The mean residual correlation ( $\pm$  standard deviation) across all thirteen MZ pairs was 0.2377 ( $\pm$  0.3013) in the left visual cortex, 0.1151 ( $\pm$  0.3033) in the right visual cortex, and 0.1510 ( $\pm$  0.2628) in the left motor cortex. The mean residual correlation across all eleven DZ pairs was -0.0421 ( $\pm$  0.2960) in the left visual cortex, -0.0734 ( $\pm$  0.2780) in the right visual cortex, and 0.0523 ( $\pm$  0.3028) in the left motor cortex. Slightly positive residual correlation on average in MZ pairs indicates that some covarying information may not have been captured by the given basis volumes. This is empirically plausible since the basis set from nineteen singleton participants might not contain enough spatial structure to capture all possible similarity between siblings. Ideally, the basis volumes should be created from a larger sample. Not being able to capture a small amount of covariance structure in MZ pairs results in underestimation of the covariance for MZ pairs. Any significant effects of genetics are therefore still significant; but the analysis becomes somewhat conservative in assessing heritability.

## Results

We first examined the activation and variability measures within the bilateral visual cortex separately in the twins and in the independent group of subjects. The group-level activation map constructed from a univariate one-sample t-test across twins was moderately correlated with the group-level activation map constructed from an independent group of nineteen subjects in all ROI's ( $r = 0.519$  in the left visual cortex,  $r = 0.561$  in the right visual cortex, and  $r = 0.507$  in the left motor cortex) (Fig. 2). The variability map constructed from a univariate standard deviation measures across twins was also highly correlated with the variability map constructed from an independent group of nineteen subjects in all ROI's ( $r = 0.793$  in the left visual cortex,  $r = 0.784$  in the right visual cortex, and  $r = 0.763$  in the left motor cortex) (Fig. 2). High similarity between the activation and variability maps from these two groups of subjects suggests that the activation maps from the singleton subjects can be used as a representative sample of the population of interest.

**Intraclass Correlation Differences**—We then examined genetic influences on neural activity in the left and right visual cortex as well as the left motor cortex using the proposed spatial decomposition method, the voxelwise method, and the mean-ROI method. In the spatial decomposition method, ICC's for MZ and DZ pairs were estimated first by estimating volume coefficients in the model (Eq. 1) and then by transforming the variance and covariance of these coefficients in the basis space onto the voxel space (Eq. 2 to 4). Table 1 summarizes results from these three methods. Figure 3 shows the ICC difference map computed using the spatial decomposition method and the voxelwise method displaying suprathreshold clusters that exceed clusterwise correction for multiple comparisons. The spatial decomposition approach identified two suprathreshold clusters in the left visual cortex one suprathreshold cluster in the right visual cortex, and one suprathreshold cluster in the left motor cortex (red clusters in Fig. 3). All three clusters were statistically significant in terms of cluster size (see Table 1).

The conventional voxelwise method identified four suprathreshold clusters in the left visual cortex and one suprathreshold cluster in the left motor, all of which were statistically significant in terms of cluster size (blue clusters in Fig. 3). However, it failed to find any clusters in the right visual cortex that reached statistical significance in cluster size at the alpha level of 0.05 (Table 1).<sup>10</sup> The range of the voxelwise ICC difference measures was also more variable than the results from the spatial decomposition method in both hemispheres (Fig. 4). The correlation across voxels between the results from the spatial decomposition method and the voxelwise method was 0.7068 in the left visual cortex, 0.5714 in the right visual cortex, and 0.6613 in the left motor cortex (Fig. 4).

The mean-ROI method found a significant difference between MZ ICC and DZ ICC in the left visual cortex ( $p = 0.0016$ ) and the left motor cortex ( $p = 0.0149$ ) overall (Table 1). In the right visual cortex, the difference just failed to reach significance ( $p = 0.0513$ ).

**Heritability**—Using the maximum-likelihood model fitting method implemented in Mx, heritability of the neural activity was estimated using three different methods. Table 2 summarizes results from the spatial decomposition method, the voxelwise method, and the mean-ROI method. Figure 5 shows the heritability map computed using the spatial decomposition method displaying suprathreshold clusters that exceed clusterwise correction for multiple comparisons. As in the case of the ICC difference measure, two suprathreshold clusters were identified in the left visual cortex, one of which was statistically significant in terms of cluster size. Additionally, one suprathreshold cluster in the left motor cortex was statistically significant in terms of cluster size.

Heritability was also estimated using the voxelwise method. None of the suprathreshold clusters in any of the three ROIs reached statistical significance (see Table 2; no blue clusters in Fig. 5).<sup>11</sup> The correlation across voxels between the results from the spatial decomposition method and the voxelwise method was 0.7437 in the left visual cortex, 0.5691 in the right visual cortex, and 0.6222 in the left motor cortex (Fig. 6).

The mean-ROI method showed that the average neural activity in the left visual cortex was significantly heritable ( $h^2 = 0.7218$ ,  $p = 0.048$ ), but no other ROI's were shown to be heritable at the alpha level 0.05.

## Discussion

In this work, we developed a statistical method to estimate correlation between related subjects at each location of a spatial process. The feasibility and the relative advantage of this spatial decomposition method over conventional methods were demonstrated using a simulation study. Correlation estimates from the spatial decomposition method had lower variance and bias compared to estimates from the voxelwise or the mean-ROI approach. This discrepancy between the RMSE from the spatial decomposition method and that from the two other conventional methods tended to be greater as the overall noise increased. These results collectively suggest that the spatial decomposition method has better control over noise than the conventional methods.

---

<sup>10</sup>Examination of cluster size significance was also performed using varying magnitude threshold. In general, clusters identified from the spatial decomposition method showed greater statistical significance than clusters identified from the voxelwise method. See Supplementary Figure S7 for further details.

<sup>11</sup>As in the ICC difference measures, examination of the cluster size significance was also performed using varying magnitude threshold. Clusters identified from the spatial decomposition method showed greater statistical significance than clusters identified from the voxelwise method. See Supplementary Figure S8 for further details.

Using a real fMRI dataset from a twin study, we then applied the spatial decomposition method to assess the genetic influence and heritability of brain activation in the primary visual and motor cortex during a simple visuomotor task. The results from the spatial decomposition method showed greater statistical significance, compared to the results from the voxelwise and the mean-ROI methods, both in the measure of ICC difference and in the measure of heritability. The left visual cortex showed greater genetic influence both in terms of magnitude and statistical significance than the right visual cortex.

In general, ICC difference and heritability estimates from the spatial decomposition method were less variable than the voxelwise method, as expected. Along with the results from the simulation study, the proposed method showed greater power in realistic settings compared to the voxelwise and mean-ROI approaches. The spatial decomposition method controls the noise by using spatial basis volumes. In a way, the voxelwise method can be considered to be a special case of the spatial decomposition method. If the number of basis volumes is equal to the number of voxels in the ROI (e.g. imagine a basis set of an identity matrix), the spatial decomposition method becomes identical to the voxelwise approach. On the other hand, if a single constant map is used as a basis volume then the spatial decomposition method is conceptually similar, although not identical, to the mean-ROI method.

In the proposed spatial decomposition method, we used an independent set of data to construct the basis volumes for the given neural activation pattern. Since the basis volumes were limited to nineteen (the number of independent group of subjects), our model could have been underspecified especially when we tried to capture over 700 voxels in each mask. Underspecification of the model results in bias towards zero, that results in a conservative assessment of genetic influence (see Simulation Study). It is also possible that the spatial variation in twin data is highly distinct from the activation patterns that can be spanned by the basis volumes. This case can be referred to as having a misspecified model as opposed to an underspecified model. In a misspecified model, spatial covariation between twins will not be captured by the basis volumes, reducing the covariance estimate (Eq. 3). The variance, however, will not be as influenced since those that cannot be captured by the basis volumes will be captured as error variance  $\sigma^2$  (see Eq. 2). Thus, as in the case of an underspecified model, a potential misspecification is also likely to result in a conservative bias in correlation estimation. Note, however, that the spatial decomposition method was better at detecting heritability than the other conventional methods in the three ROIs in the real data study<sup>12</sup>.

Nonetheless, an adequate construction of the basis volumes can improve the model even further. One potential method is to use either functional localizer data or images from orthogonal contrasts (Berman et al., 2010; Friston et al., 2006; Saxe et al., 2006) as independent datasets to construct the basis volumes. This way, there is no need to collect data from independent subjects and it will result in a much larger basis set given that modern fMRI twin studies have a few tens, if not hundreds, of subjects.

Additionally, other ways to construct a set of basis volumes may be considered. For instance, independent component analysis, based on complete independence or lack of association in the higher-order moments, is another possible approach for constructing a

---

<sup>12</sup>The exact same analyses were also performed in the whole brain. After heritability estimation using an AE model and setting the magnitude threshold as the 99 percentile of the entire  $h^2$  range, 81 suprathreshold clusters were identified from the voxelwise method and 8 suprathreshold clusters were identified from the spatial decomposition method. After 200 repetitions using the permutation scheme, the cluster size significance of the largest cluster identified from the voxelwise method was  $p=0.485$  and the cluster size significance of the largest cluster identified from the voxelwise method was  $p=0.100$ . These results demonstrate that the spatial decomposition method, even though it may be extremely underspecified to capture the spatial dependencies of the whole brain, is more powerful than the voxelwise method.

meaningful basis set. Since heritability is defined in terms of second-order moments (variance and covariance), it is important to construct spatial variation that best captures the variance of the spatial pattern. We, therefore, used a singular value decomposition approach in this work. Nevertheless, it would be an interesting future work to explore how basis volumes derived from other approaches could be applied to the proposed spatial decomposition method.

There has been some recent advance in the heritability estimation in diffusion tensor imaging data (Brun et al., 2009; Jahanshad et al., 2010) and genetic covariance estimation in structural imaging data (Schmitt et al., 2007). While these studies incorporate multivariate statistical analyses in heritability estimation, our study is quite different in a number of ways. The goal of our work is to borrow information from neighboring voxels to improve the precision of voxelwise heritability estimates. This is particularly a critical issue in functional neuroimaging studies, as the noise level is substantially higher than in the structural studies. In addition, recent research in functional neuroimaging has started to emphasize the spatial and network-like nature of brain activity. Many studies have demonstrated that information is encoded over a large number of brain regions in a distributed and overlapping fashion (Haynes & Rees, 2006; Norman et al., 2007). In addition, many studies have shown that multiple brain regions are intrinsically organized into networks (Achard et al., 2006; Greicius et al., 2003) so that analyzing the functional role of a particular brain region may be impossible without considering other regions. It is therefore important to understand and consider the spatial dependencies in patterns of brain activation when estimating the heritability of such patterns.

In summary, we developed a statistical method to estimate correlation and heritability at each position in a spatial dataset. We then applied this method to assess the influence of genetics on the pattern of neural activities evoked by a visuomotor task. The proposed spatial decomposition method was shown to be more efficient than the conventional voxelwise and mean-ROI methods in our experiments. The results also showed that neural activity evoked by a simple visuomotor task is under significant genetic influence particularly in the left visual cortex and the left motor cortex.

## Supplementary Material

Refer to Web version on PubMed Central for supplementary material.

## Appendix

### Fisher's ICC

Given  $N$  paired data values  $(x_{n1}, x_{n2})$  where  $n=1 \dots N$ , the following defines Fisher's ICC (Fisher, 1954):

$$\begin{aligned}\bar{x} &= \frac{1}{2N} \sum_{n=1}^N (x_{n1} + x_{n2}), \\ \text{cov}(x_{\bullet 1}, x_{\bullet 2}) &= \frac{1}{N-1} \sum_{n=1}^N (x_{n1} - \bar{x})(x_{n2} - \bar{x}), \\ \text{var}(x_{\bullet \bullet}) &= \frac{1}{2N-1} \left( \sum_{n=1}^N (x_{n1} - \bar{x})^2 + \sum_{n=1}^N (x_{n2} - \bar{x})^2 \right), \\ \text{ICC}(x_{\bullet 1}, x_{\bullet 2}) &= \frac{\text{cov}(x_{\bullet 1}, x_{\bullet 2})}{\text{var}(x_{\bullet \bullet})}.\end{aligned}$$

### Bias correction for the plug-in estimates

The estimators we use follow standard approaches from fixed effects modeling (Allison, 2005; Robinson, 1991; Searle et al., 1992). The bias correction procedure was adopted because the sample variance of the estimated fixed effects is biased due to uncertainty in the fixed effects estimates. The adjustment we use removes this bias. The variance and covariance ( $\hat{\text{var}}(\beta_{p\bullet\bullet})$  and  $\hat{\text{cov}}(\beta_{p\bullet 1}, \beta_{p\bullet 2})$ ) of the random effects can be estimated starting from the empirical variance and covariance of the fitted fixed effects ( $\text{var}(\hat{\beta}_{p\bullet\bullet})$  and  $\text{cov}(\hat{\beta}_{p\bullet 1}, \hat{\beta}_{p\bullet 2})$ ). The empirical estimates are subject to a bias correction:

$$\text{var}(\hat{\beta}) = \frac{1}{2n-1} \sum_i^{2n} (\hat{\beta}_i - \bar{\hat{\beta}})^2 = \frac{1}{2n-1} (Q \hat{\beta})' (Q \hat{\beta}) = \frac{1}{2n-1} \hat{\beta}' Q \hat{\beta}$$

where  $Q$  is an idempotent centering matrix. Matrix  $Q$  can be constructed so that the above equation can yield  $\text{var}(\hat{\beta}_{p\bullet 1})$ ,  $\text{var}(\hat{\beta}_{p\bullet 2})$ , or pooled variance  $\hat{\text{var}}\beta_{\bullet\bullet}$  to be used for intraclass correlation.

Taking the expected value,

$$\begin{aligned} E\left(\frac{1}{2n-1} \hat{\beta}' Q \hat{\beta}\right) &= \frac{1}{2n-1} \text{tr}\left(Q \cdot E\left(\hat{\beta}\hat{\beta}'\right)\right) = \frac{1}{2n-1} \text{tr}\left(Q \cdot \left[(X'X)^{-1}\sigma^2 + \beta\beta'\right]\right) \\ &= \frac{1}{2n-1} \text{tr}\left(Q(X'X)^{-1}\sigma^2\right) + \frac{1}{2n-1} \text{tr}(Q\beta\beta') = \frac{1}{2n-1} \text{tr}\left(Q(X'X)^{-1}\sigma^2\right) + \frac{1}{2n-1} \beta' Q \beta \end{aligned}$$

Thus, the term  $\frac{1}{2n-1} \text{tr}\left(Q(X'X)^{-1}\sigma^2\right)$  can be subtracted from the plug-in estimates to correct for bias.

Likewise,

$$\text{cov}\left(\hat{\beta}_1, \hat{\beta}_2\right) = \frac{1}{n-1} (Q_1 \hat{\beta})' (Q_2 \hat{\beta}) = \frac{1}{n-1} \hat{\beta}' Q_1' Q_2 \hat{\beta} = \frac{1}{n-1} \text{tr}\left(Q_1' Q_2 \hat{\beta}\hat{\beta}'\right)$$

where  $n$ -by- $2n$  matrices  $Q_1$  and  $Q_2$  represent a centering matrix. Matrices  $Q_1$  and  $Q_2$  can be constructed so that the above equation can either yield interclass covariance or intraclass covariance.

Taking the expected value,

$$\begin{aligned} E\left(\frac{1}{n-1} \text{tr}\left(Q_1' Q_2 \hat{\beta}\hat{\beta}'\right)\right) &= \frac{1}{n-1} \text{tr}\left(Q_1' Q_2 (X'X)^{-1}\sigma^2\right) + \frac{1}{n-1} \text{tr}\left(Q_1' Q_2 \beta\beta'\right) \\ &= \frac{1}{n-1} \text{tr}\left(Q_1' Q_2 (X'X)^{-1}\sigma^2\right) + \frac{1}{n-1} (Q_1 \beta)' (Q_2 \beta) \end{aligned}$$

Thus, the bias  $\frac{1}{n-1} \text{tr}\left(Q_1' Q_2 (X'X)^{-1}\sigma^2\right)$  can be subtracted from the plug-in estimates to correct for bias.

## References

- Achard S, Salvador R, Whitcher B, Suckling J, Bullmore E. A resilient, low-frequency, small-world human brain functional network with highly connected association cortical hubs. *Journal of Neuroscience*. 2006; 26:63–72. [PubMed: 16399673]
- Allison, P. *Fixed Effects Regression Methods for Longitudinal Data Using SAS*. SAS Publisher; 2005.
- Berman MG, Park J, Gonzalez R, Polk TA, Gehrke A, Knaffla S, Jonides J. Evaluating functional localizers: the case of the FFA. *Neuroimage*. 2010; 50:56–71. [PubMed: 20025980]
- Blokland GAM, McMahon KL, Hoffman J, Zhu G, Meredith M, Martin NG, Thompson PM, de Zubicaray GI, Wright MJ. Quantifying the heritability of task-related brain activation and performance during the N-back working memory task: A twin fMRI study. *Biological Psychology*. 2008; 79:70–79. [PubMed: 18423837]
- Brun CC, Lepore N, Pennec X, Lee AD, Barysheva M, Madsen SK, Avedissian C, Chou YY, de Zubicaray GI, McMahon KL, Wright MJ, Toga AW, Thompson PM. Mapping the regional influence of genetics on brain structure variability - A Tensor-Based Morphometry study. *Neuroimage*. 2009; 48:37–49. [PubMed: 19446645]
- Chiang, MC.; Barysheva, M.; Lee, AD.; Madsen, S.; Klunder, AD.; Toga, AW.; McMahon, KL.; de Zubicaray, GI.; Meredith, M.; Wriqh, MJ.; Srivastava, A.; Balov, N.; Thompson, PM. Mapping genetic influences on brain fiber architecture with high angular resolution diffusion imaging (HARDI). 2008 Ieee International Symposium on Biomedical Imaging: From Nano to Macro; 2008. p. 871-874.
- Cote C, Beauregard M, Girard A, Mensour B, Mancini-Marie A, Perusse D. Individual variation in neural correlates of sadness in children: A twin fMRI study. *Human Brain Mapping*. 2007; 28:482–487. [PubMed: 17437293]
- Falconer, DS.; Mackay, TFC. *Introduction to Quantitative Genetics*. Longmans Green; Harlow, Essex, UK: 1996. p. 160-183.
- Fisher, RA. *Statistical Methods for Research Workers*. 12th. Oliver and Boyd; 1954.
- Friston KJ, Rotshtein P, Geng JJ, Sterzer P, Henson RN. A critique of functional localisers. *Neuroimage*. 2006; 30:1077–1087. [PubMed: 16635579]
- Greicius MD, Krasnow B, Reiss AL, Menon V. Functional connectivity in the resting brain: A network analysis of the default mode hypothesis. *Proceedings of the National Academy of Sciences of the United States of America*. 2003; 100:253–258. [PubMed: 12506194]
- Haynes JD, Rees G. Decoding mental states from brain activity in humans. *Nature Reviews Neuroscience*. 2006; 7:523–534.
- Holmes AP, Blair RC, Watson JDG, Ford I. Nonparametric analysis of statistic images from functional mapping experiments. *Journal of Cerebral Blood Flow and Metabolism*. 1996; 16:7–22. [PubMed: 8530558]
- Huettel, SA.; Song, AW.; Gregory, M. *Functional Magnetic Resonance Imaging*. Sinauer Associates, Inc.; Sunderland, MA: 2004. p. 217-251.
- Jahanshad N, Lee AD, Barysheva M, McMahon KL, de Zubicaray GI, Martin NG, Wright MJ, Toga AW, Thompson PM. Genetic influences on brain asymmetry: A DTI study of 374 twins and siblings. *Neuroimage*. 2010; 52:455–469. [PubMed: 20430102]
- Koten JW, Wood G, Hagoort P, Goebel R, Propping P, Willmes K, Boomsma DI. Genetic Contribution to Variation in Cognitive Function: An fMRI Study in Twins. *Science*. 2009; 323:1737–1740. [PubMed: 19325117]
- Maldjian JA, Laurienti PJ, Burdette JB, Kraft RA. An Automated Method for Neuroanatomic and Cytoarchitectonic Atlas-based Interrogation of fMRI Data Sets. *NeuroImage*. 2003; 19:1233–1239. [PubMed: 12880848]
- Matthews SC, Simmons AN, Strigo I, Jang K, Stein MB, Paulus MP. Heritability of anterior cingulate response to conflict: An fMRI study in female twins. *Neuroimage*. 2007; 38:223–227. [PubMed: 17707125]
- Neale, MC. Twin analysis. In: Armitage, P.; Colton, T., editors. *Encyclopedia of Biostatistics*. John Wiley; New York: 1998.

- Neale, MC. Twin studies: Software and algorithms. In: Cooper, DN., editor. *Encyclopedia of the Human Genome*. Macmillan Publishers Ltd.; 2003.
- Neale, M.; Boker, SM.; Xie, G.; Maes, H. *Mx Statistical Modeling*. Medical College of Virginia; 2003.
- Nichols TE, Holmes AP. Nonparametric permutation tests for functional neuroimaging: A primer with examples. *Human Brain Mapping*. 2002; 15:1–25. [PubMed: 11747097]
- Norman KA, Polyn SM, Detre GJ, Haxby JV. Beyond mind-reading: multi-voxel pattern analysis of fMRI data. *Trends in Cognitive Sciences*. 2006; 10:424–430. [PubMed: 16899397]
- Polk TA, Park J, Smith MR, Park DC. Nature versus nurture in ventral visual cortex: A functional magnetic resonance Imaging study of twins. *Journal of Neuroscience*. 2007; 27:13921–13925. [PubMed: 18094229]
- Robinson GK. That BLUP is a Good Thing: The Estimation of Random Effects. *Statistical Science*. 1991; 6:15–32.
- Saxe R, Brett M, Kanwisher N. Divide and conquer: A defense of functional localizers. *Neuroimage*. 2006; 30:1088–1096. [PubMed: 16635578]
- Schmitt JE, Wallace GL, Rosenthal MA, Molloy EA, Ordaz S, Lenroot R, Clasen LS, Blumenthal JD, Kendler KS, Neale MC, Giedd JN. A multivariate analysis of neuroanatomic relationships in a genetically informative pediatric sample. *Neuroimage*. 2007; 35:70–82. [PubMed: 17208460]
- Schmitt JE, Lenroot RK, Ordaz SE, Wallace GL, Lerch JP, Evans AC, Prom EC, Kendler KS, Neale MC, Giedd JN. Variance decomposition of MRI-based covariance maps using genetically informative samples and structural equation modeling. *Neuroimage*. 2009; 47:56–64. [PubMed: 18672072]
- Searle, SR.; Casella, G.; McCulloch, CE. *Variance Components*. John Wiley & Sons, Inc.; 2008.
- Stuart, A.; Ord, K. *Kendall's Advanced Theory of Statistics*. Wiley; 2009. p. 351
- Thompson PM, Cannon TD, Narr KL, van Erp T, Poutanen VP, Huttunen M, Lonnqvist J, Standertskjold-Nordenstam CG, Kaprio J, Khaledy M, Dail R, Zoumalan CI, Toga AW. Genetic influences on brain structure. *Nature Neuroscience*. 2001; 4:1253–1258.
- Tzourio-Mazoyer N, Landeau B, Papathanassiou D, Crivello F, Etard O, Delcroix N, Mazoyer B, Joliot M. Automated anatomical labeling of activations in SPM using amacroscopic anatomical parcellation of the MNI MRI single-subject brain. *Neuroimage*. 2002; 15(1):273–89. [PubMed: 11771995]

### Research Highlights

- A statistical method is developed to estimate correlation of spatial data.
- Provides ways to account for spatial dependencies in neural activation.
- Advantages over existing methods for estimating heritability of spatial traits.
- Heritable neural patterns for simple visuomotor processing are identified.

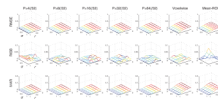


**Figure 1.**

Results of the simulation study using the proposed spatial decomposition method (columns 1-5), the voxelwise method (column 6), and the mean-ROI method (column 7) with 20 pairs. Patterns of neural activation for twin pairs were simulated with 32 basis volumes while varying the degree of correlation between pairs ( $r$ ) and the error variability ( $\sigma$ ). The estimated correlation was compared with the true correlation, and root mean squared error (RMSE), root integrated squared bias (RISB), and integrated variance (IVAR) were computed over the parameter space. In the case of the spatial decomposition method, the correlation was estimated using a subset of basis volumes (4, 8, or 16, as represented in the first three columns), all 32 basis volumes (represented in the fourth column), and 64 basis volumes (represented in the fifth column). See Supplementary Figures for cases of  $N=10$  and  $N=40$ .

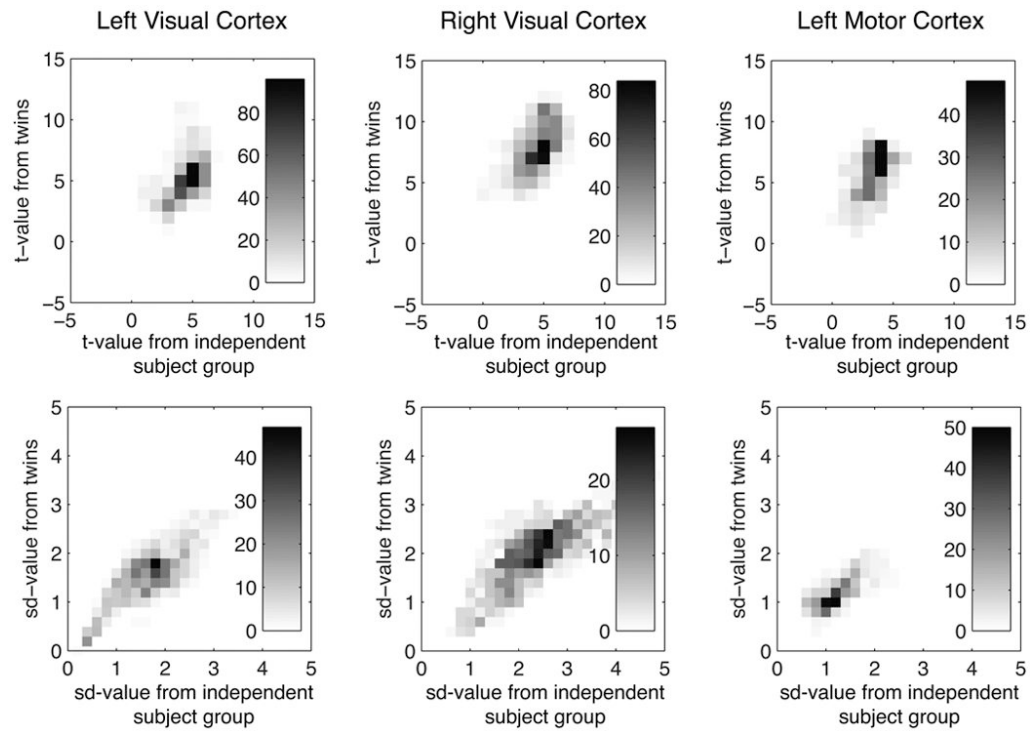


**Figure 2.**

Density plots for the activation map and variability map computed from two groups of subjects. Group-level one-sample t-maps and standard deviation (sd) maps were constructed from twins in the left and right visual cortex and the left motor cortex. These maps were then compared against the t-maps and sd-maps from the independent group of subjects. The plots indicate the number of voxels that exhibited a specific statistical value in both groups of subjects.

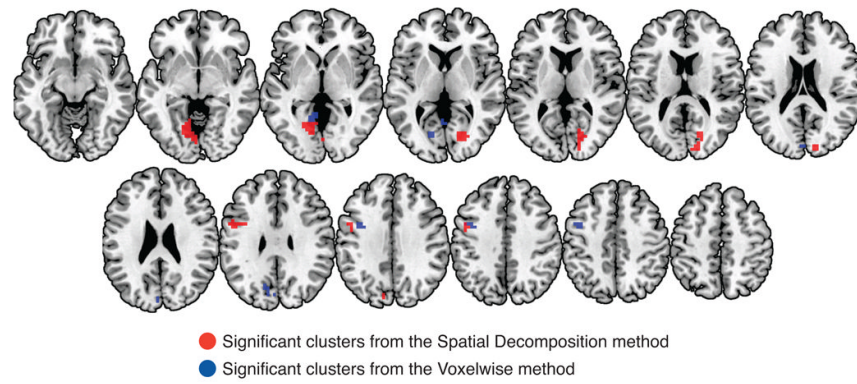


**Figure 3.**

Map of ICC difference estimated from the spatial decomposition (red) and the voxelwise (blue) methods. Only statistically significant clusters ( $p < 0.05$  using clusterwise correction for multiple comparisons incorporating permutation with a magnitude threshold of 95 percentile) are overlaid on a canonical brain in MNI space with axial slices from  $z = -10$  to  $z = 50$  in increments of 5 mm. The left hemisphere appears on the left for all brain images.

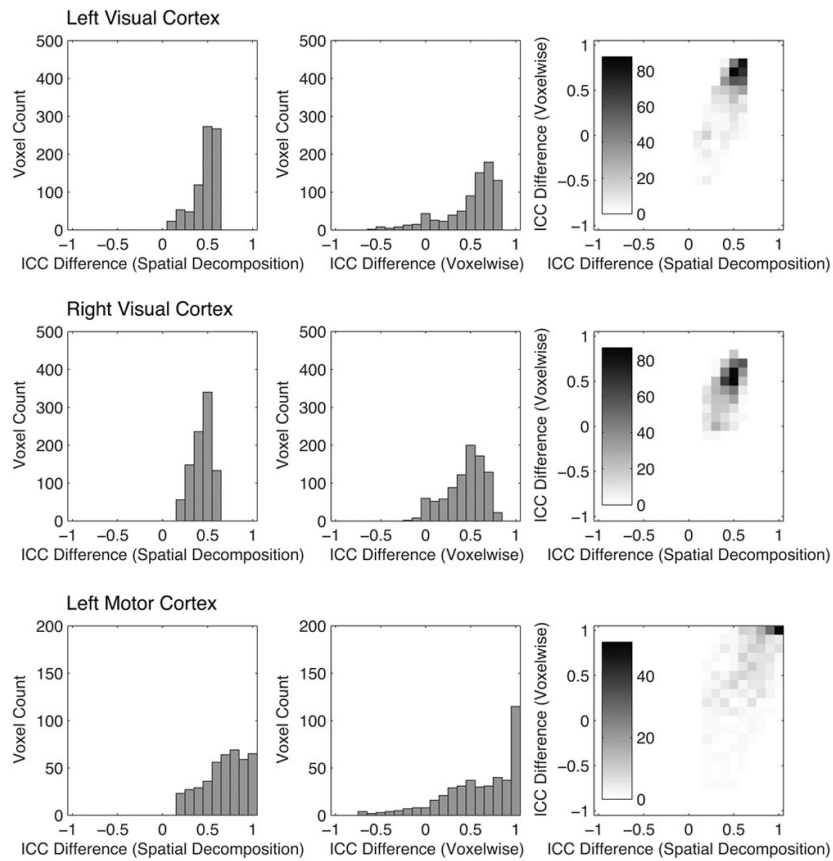


**Figure 4.** Histograms of ICC difference in the left and right visual cortex estimated from the spatial decomposition method and the voxelwise method, as well as the joint histogram of ICC difference estimates between the two methods across the whole brain.

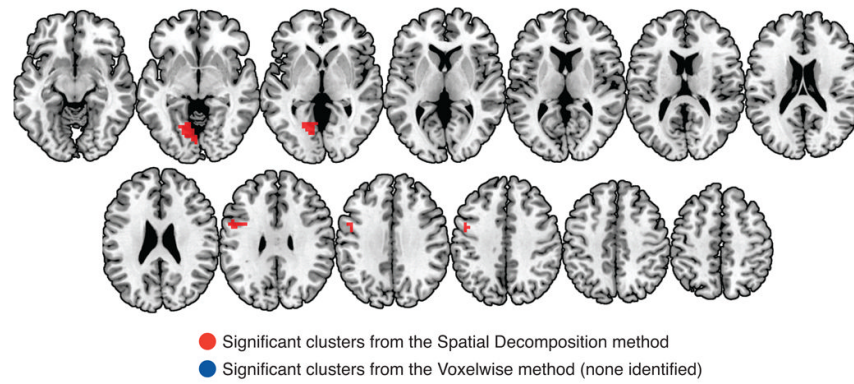


**Figure 5.**

Map of heritability ( $h^2$ ) estimated from the spatial decomposition method. Only statistically significant clusters ( $p < 0.05$  using clusterwise correction for multiple comparisons incorporating permutation with a magnitude threshold of 95 percentile) are overlaid on a canonical brain in MNI space with axial slices from  $z = -10$  to  $z = 50$  in increments of 5 mm. None of the clusters identified from the voxelwise method was statistically significant.

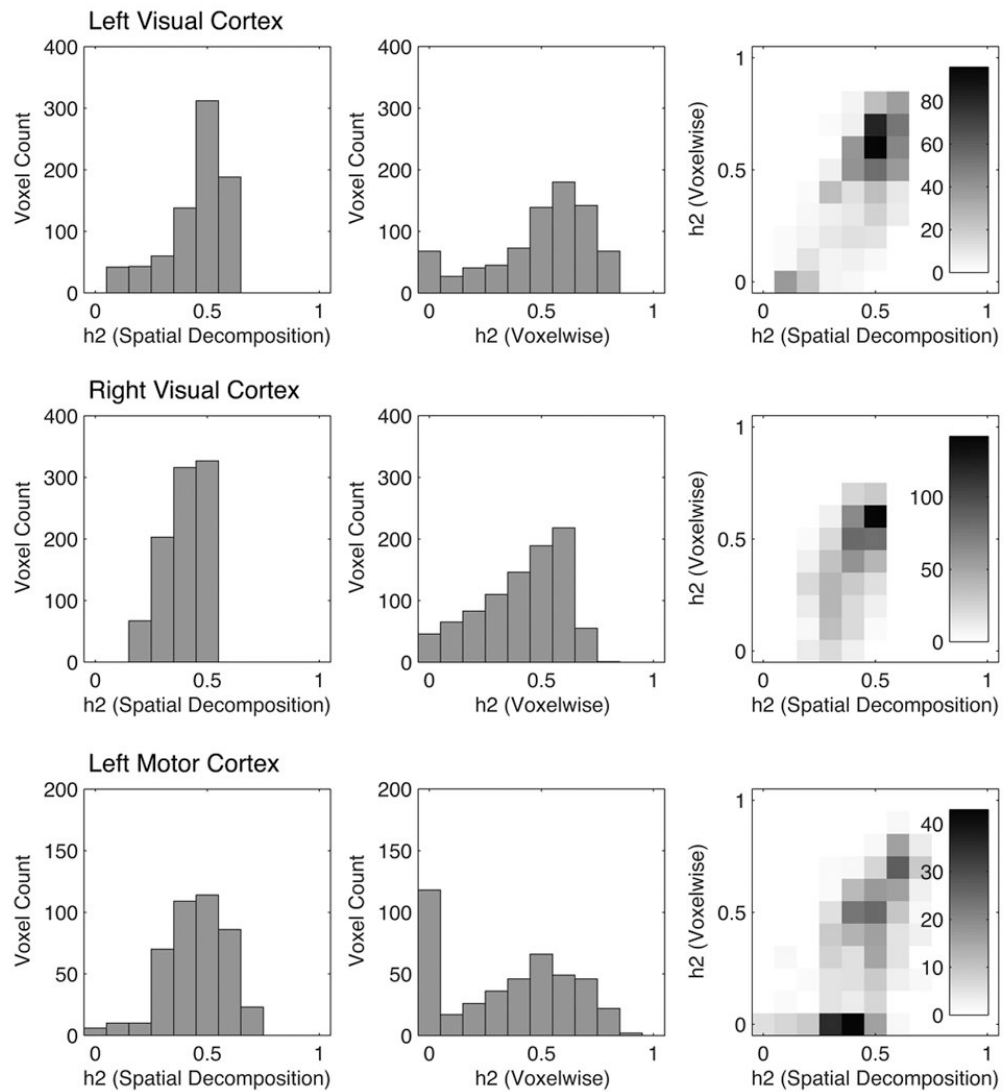


**Figure 6.** Histograms of heritability ( $h^2$ ) in the left and right visual cortex estimated from the spatial decomposition method and the voxelwise method, as well as the joint histogram of  $h^2$  estimates between the two methods across the whole brain.

Table 1

Cluster analysis of the ICC difference map estimated from the spatial decomposition method and the voxelwise method, and mean ICC difference value from the mean-ROI method.

ROI	Method	Magnitude threshold (95 percentile)	Cluster threshold ( $p < 0.05$ )	Cluster sizes (p-values)	Mean ICC Difference (p-value)
Left Visual Cortex	Spatial Decomposition	0.6206	0 voxels	36 voxels ( $p=0.0020$ ) 4 voxels ( $p=0.0055$ )	-
	Voxelwise	0.7998	3 voxels	23 voxels ( $p=0.0023$ ) 4 voxels ( $p=0.0329$ ) 6 voxels ( $p=0.0223$ ) 7 voxels ( $p=0.0190$ )	-
	Mean-ROI	-	-	-	0.7264 ( $p=0.0016$ ),
Right Visual Cortex	Spatial Decomposition	0.5763	0 voxels	46 ( $p=0.0183$ )	-
	Voxelwise	0.7235	28 voxels	1 voxel ( $p=0.3155$ ) 18 voxels ( $p=0.0792$ ) 1 voxel ( $p=0.3155$ ) 26 voxels ( $p=0.0536$ )	-
	Mean-ROI	-	-	-	0.5808 ( $p=0.0513$ ),
Left Motor Cortex	Spatial Decomposition	0.7457	0 voxels	22 ( $p=0.0022$ )	-
	Voxelwise	0.8467	2 voxels	22 ( $p=0.0021$ )	-
	Mean-ROI	-	-	-	0.8446 ( $p=0.0149$ )

**Table 2**

Cluster analysis of the heritability map estimated from the spatial decomposition method and the voxelwise method, and mean ICC difference value from the mean-ROI method.

ROI	Method	Magnitude threshold (95 percentile)	Cluster threshold ( $p < 0.05$ )	Cluster sizes (p-values)	Heritability (p-value)
Left Visual Cortex	Spatial Decomposition	0.6055	11 voxels	36 voxels ( $p=0.028$ ) 4 voxels ( $p=0.058$ )	-
	Voxelwise	0.7780	46 voxels	33 voxels ( $p=0.096$ ) 7 voxels ( $p=0.458$ )	-
	Mean-ROI	-	-	-	0.7218 ( $p=0.048$ )
Right Visual Cortex	Spatial Decomposition	0.5262	70 voxels	46 voxels ( $p=0.070$ )	-
	Voxelwise	0.6570	145 voxels	1 voxel ( $p=0.949$ ) 8 voxels ( $p=0.831$ ) 4 voxel ( $p=0.903$ ) 33 voxels ( $p=0.556$ )	-
	Mean-ROI	-	-	-	0.5551 ( $p=0.096$ )
Left Motor Cortex	Spatial Decomposition	0.6509	16 voxels	22 voxels ( $p = 0.044$ )	-
	Voxelwise	0.7784	31 voxels	20 voxels ( $p = 0.122$ ) 2 voxel ( $p = 0.571$ )	-
	Mean-ROI	-	-	-	0.7451 ( $p=0.123$ )